Revealing the time-dependent polarization of ultrashort pulses with sub-cycle resolution

R. Boge,[1,*] **S. Heuser,**[1] **M. Sabbar,**[1] **M. Lucchini,**[1] **L. Gallmann,**[1,2]
C. Cirelli,[1] **and U. Keller**[1]

[1]*Department of Physics, Institute for Quantum Electronics, ETH Zurich, 8093 Zurich, Switzerland*
[2]*Institute of Applied Physics, University of Bern, 3012 Bern, Switzerland*
[*]*rboge@phys.ethz.ch*

Abstract: We report on the first experiments characterizing the complete time-dependent 2D vector potential of a few-cycle laser pulse. The instantaneous amplitude and orientation of the electric field is determined with sub-cycle resolution, directly giving access to the polarization state of the pulse at any instant in time. This is achieved by performing an attosecond streaking experiment using a reaction microscope, where the full pulse characterization is performed directly in the target region.

References and links

1. F. Krausz and M. Ivanov, "Attosecond physics," Rev. Mod. Phys. **81**(1), 163 (2009).
2. G. Steinmeyer, D. H. Sutter, L. Gallmann, N. Matuschek, and U. Keller, "Frontiers in ultrashort pulse generation: pushing the limits in linear and nonlinear optics," Science **286**(5444), 1507–1512 (1999).
3. I. A. Walmsley and C. Dorrer, "Characterization of ultrashort electromagnetic pulses," Adv. Opt. Photon. **1**(2), 308–437 (2009).
4. C. Iaconis and I. A. Walmsley, "Self-referencing spectral interferometry for measuring ultrashort optical pulses," IEEE J. Quantum Electron. **35**(4), 501–509 (1999).
5. R. Trebino, K. W. DeLong, D. N. Fittinghoff, J. N. Sweetser, M. A. Krumbgel, B. A. Richman, and D. J. Kane, "Measuring ultrashort laser pulses in the time-frequency domain using frequency-resolved optical gating," Rev. Sci. Instrum. **68**(9), 3277–3295 (1997).
6. H. R. Telle, G. Steinmeyer, A. E. Dunlop, J. Stenger, D. H. Sutter, and U. Keller, "Carrier-envelope offset phase control: A novel concept for absolute optical frequency measurement and ultrashort pulse generation," Appl. Phys. B **69**(4), 327–332 (1999).
7. L. Gallmann, D. H. Sutter, N. Matuschek, G. Steinmeyer, U. Keller, C. Iaconis, and I. A. Walmsley, "Characterization of sub-6-fs optical pulses with spectral phase interferometry for direct electric-field reconstruction," Opt. Lett. **24**(18), 1314-1316 (1999).
8. L. Gallmann, D. H. Sutter, N. Matuschek, G. Steinmeyer, and U.Keller, "Techniques for the characterization of sub-10-fs optical pulses: a comparison," Appl. Phys. B **70**(1), 67–75 (2000).
9. L. Gallmann, G. Steinmeyer, D. H. Sutter, T. Rupp, C. Iaconis, I. A. Walmsley, and U. Keller, "Spatially resolved amplitude and phase characterization of femtosecond optical pulses," Opt. Lett. **26**(2), 96–98 (2001).
10. G. G. Paulus, F. Grasbon, H. Walther, P. Villoresi, M. Nisoli, S. Stagira, E. Priori, and S. De Silvestri, "Absolute-phase phenomena in photoionization with few-cycle laser pulses," Nature **414**(6860), 182–184 (2001).
11. G. G. Paulus, F. Lindner, H. Walther, A. Baltuška, E. Goulielmakis, M. Lezius, and F. Krausz, "Measurement of the phase of few-cycle laser pulses," Phys. Rev. Lett. **91**(25), 253004 (2003).
12. J. Itatani, F. Quéré, G. L. Yudin, M. Y. Ivanov, F. Krausz, and P. B. Corkum, "Attosecond streak camera, "Phys. Rev. Lett. **88**(17), 173903 (2002).

13. R. Kienberger, E. Goulielmakis, M.Uiberacker, A. Baltuška, V. Yakovlev, F. Bammer, A. Scrinzi, T. Wester-walbesloh, U. Kleineberg, U. Heinzmann, M. Drescher, and F. Krausz, "Atomic transient recorder," Nature **427**(6977), 817–821 (2004).

14. P. Eckle, M. Smolarski, P. Schlup, J. Biegert, A. Staudte, M. Schöffler, H. G. Muller, R. Dörner, and U.Keller, "Attosecond angular streaking," Nat. Phys. **4**(7), 565–570 (2008).

15. P. Eckle, A. N. Pfeiffer, C. Cirelli, A. Staudte, R. Dörner, H. G. Muller, M. Büttiker, and U. Keller, "Attosecond ionization and tunneling delay time measurements in helium," Science **322**(5907), 1525–1529 (2008).

16. W. J. Walecki, D. N. Fittinghoff, A. L. Smirl, and Rick Trebino, "Characterization of the polarization state of weak ultrashort coherent signals by dual-channel spectral interferometry," Opt. Lett. **22**(2), 81–83 (1997).

17. T. Brixner, G. Krampert, T. Pfeifer, R. Selle, G. Gerber, M. Wollenhaupt, O. Graefe, C. Horn, D. Liese, and T. Baumert, "Quantum control by ultrafast polarization shaping," Phys. Rev. Lett. **92**(20), 208301 (2004).

18. T. Brixner, G. Krampert, P. Niklaus, and G. Gerber, "Generation and characterization of polarization-shaped femtosecond laser pulses," Appl. Phys. B **74**(1), 133–144 (2002).

19. I. J. Sola, E. Mével, L. Elouga, E. Constant, V. Strelkov, L. Poletto, P. Villoresi, E. Benedetti, J.P. Caumes, S. Stagira, C. Vozzi, M. Nisoli, and G. Sansone, "Controlling attosecond electron dynamics by phase-stabilized polarization gating," Nat. Phys. **2**(5), 319–322 (2006).

20. Y. Mairesse and F. Quéré, "Frequency-resolved optical gating for complete reconstruction of attosecond bursts," Phys. Rev. A **71**(1), 011401(2005).

21. E. Goulielmakis, M. Uiberacker, R. Kienberger, A. Baltuška, V. Yakovlev, A. Scrinzi, Th Westerwalbesloh, U. K-leineberg, U. Heinzmann, M. Drescher, and F. Krausz, "Direct measurement of light waves," Science **305**(5688), 1267–1269 (2004).

22. A. Assion, T. Baumert, M. Bergt, T. Brixner, B. Kiefer, V. Seyfried, M. Strehle, and G. Gerber, "Control of chemical reactions by feedback-optimized phase-shaped femtosecond laser pulses," Science **282**(5390), 919–922 (1998).

23. D. Meshulach and Y. Silberberg, "Coherent quantum control of two-photon transitions by a femtosecond laser pulse," Nature **396**(6708), 239–242 (1998).

24. D. M. Villeneuve, S. A. Aseyev, P. Dietrich, M. Spanner, M. Yu Ivanov, and P. B. Corkum, "Forced molecular rotation in an optical centrifuge," Phys. Rev. Lett. **85**(3), 542 (2000).

25. C. Altucci, C. Delfin, L. Roos, M. B. Gaarde, A. L'Huillier, I.Mercer, T. Starczewski, and C-G. Wahlström, "Frequency-resolved time-gated high-order harmonics," Phys. Rev. A **58**(5), 3934 (1998).

26. J. Ullrich, R. Moshammer, A. Dorn, and R. Dörner. "Recoil-ion and electron momentum spectroscopy: reaction-microscope," Rep. Prog. Phys. **66**(9), 1463–1545 (2003).

27. M. Nisoli, S. De Silvestri, O. Svelto, R. Szipöcs, K. Ferencz, C. Spielmann, S. Sartania, and F. Krausz, "Compression of high-energy laser pulses below 5 fs," Opt. Lett. **22**(8), 522 (1997).

28. M. Wollenhaupt, M. Krug, J. Köhler, T. Bayer, C. Sarpe-Tudoran, and T. Baumert, "Three-dimensional tomographic reconstruction of ultrashort free electron wave packets," Appl. Phys. B **95**(4), 647 (2009).

29. C. Smeenk, L. Arissian, A. Staudte, D. M. Villeneuve, and P. B. Corkum, "Momentum space tomographic imaging of photoelectrons," J. Phys. B **42**(18), 185402 (2009).

30. A. N. Pfeiffer, C. Cirelli, M. Smolarski, and U. Keller, "Recent attoclock measurements of strong field ionization," Chem. Phys. **414**, 84–91 (2013).

31. R. Boge, C. Cirelli, A. S. Landsman, S. Heuser, A. Ludwig, J. Maurer, M. Weger, L. Gallmann, and U. Keller, "Probing nonadiabatic effects in strong-field tunnel ionization," Phys. Rev. Lett. **111**(10), 103003 (2013).

32. R. Taïeb, V. Vniard, A. Maquet, N. L. Manakov, and S. I. Marmo, "Circular dichroism from unpolarized atoms in multiphoton multicolor ionization," Phys. Rev. A **62**(1), 013402 (2000).

33. M. Schultze, M. Fie, N. Karpowicz, Justin Gagnon, M. Korbman, M. Hofstetter, S. Neppl,A. L. Cavalieri, Y. Komninos, Th. Mercouris, C. A. Nicolaides, R. Pazourek, S. Nagele, J. Feist, J. Burgdörfer, A. M. Azzeer, R. Ernstorfer, R. Kienberger, U. Kleineberg, E. Goulielmakis, F. Krausz, and V. S. Yakovlev, "Delay in photoemission," Science **328**(5986), 1658–1662 (2010).

34. K. Klünder, J. M. Dahlström, M. Gisselbrecht, T. Fordell, M. Swoboda, D. Guénot, P. Johnsson, J. Caillat, J. Mauritsson, A. Maquet, R. Taïeb, and A. L'Huillier, "Probing single-photon ionization on the attosecond time scale," Phys. Rev. Lett. **106**(14), 143002 (2011).

35. M. Sabbar, S. Heuser, R. Boge, M. Lucchini, L. Gallmann, C. Cirelli, and U. Keller, "Attochirp-corrected photo ionization time delays using coincidence attosecond streaking," arXiv:physics.atom-ph/1407.6623.

36. A. S. Kheifets, "Time delay in valence-shell photoionization of noble-gas atoms," Phys. Rev. A **87**(6), 063404 (2013).

37. P. Antoine, Anne L'Huillier, M. Lewenstein, P. Salieères, and B. Carré, "Theory of high-order harmonic generation by an elliptically polarized laser field," Phys. Rev. A **53**(3), 1725 (1996).

1. Introduction

The development of ultrafast laser sources providing few-cycle infrared (IR) pulses in the last decades [1, 2] has called for pulse characterization methods beyond traditional autocorrelations [3]. The field envelope of linearly polarized pulses can be precisely characterized with techniques such as spectral phase interferometry for direct electric-field reconstruction (SPIDER) [4] or frequency-resolved optical gating (FROG) [5]. However, with these techniques their carrier-envelope offset (CEO) phase [6] remains undetermined. The ultrabroad spectrum of few-cycle pulses imposes additional errors [7–9] because of finite phase matching bandwidth in the nonlinear media, the bandwidth of the optics in the setup, or because the nonlinear signal cannot be cleanly separated from the fundamental spectral components anymore. The CEO phase alone can be retrieved with spectral self-referencing techniques [6] or with stereo ionization experiments [10, 11], though without providing any further information about the pulse shape. Here, we present a technique, building on the attosecond streaking techniques (such as the attosecond streak camera [12, 13] and the attoclock [14, 15]), that fully characterizes the vectorial field of the IR pulse at the target, directly where experiments are performed. The method provides amplitude and orientation of the electric field vector at any moment of the pulse with sub-cycle resolution and without imposing any limitation to the spectral range, duration, or polarization of the pulse to be characterized.

Alternative approaches to access the time-dependent polarization of a laser pulse were presented in [16–18], employing spectral interferometry. However, the pulses were not measured directly, but reconstructed, assuming the precise knowledge of a reference pulse as well as exact characterization of involved optics. Additionally, without access to the CEO phase, only the pulse envelope is characterized without resolving the vectorial laser field with sub-cycle resolution.

The technique presented here employs a completely different approach. Instead of reconstructing the spectral phase, we directly measure the vector potential of the IR pulse in the time domain with an attosecond streaking technique where the pump is a single attosecond pulse (SAP) [19] and the probe is an IR pulse. Attosecond streaking is generally used to characterize the SAP itself [20] but also provides a direct measurement of the probing IR pulse [21]. We extend the classical streaking technique, which is performed with linearly polarized IR pulses, to pulses with arbitrary, time-evolving polarization.

The precise characterization of a few-cycle IR pulse is an important prerequisite e.g. for quantum control experiments. At first, linearly polarized pulses with optimized shapes were tailored for controlling quantum systems [22, 23]. Later, this concept was generalized to pulses with time-dependent polarization states [17, 24]. In these cases, our characterization technique would allow for the full characterization of the polarization state of the pulse in the target itself, which is necessary to understand the reaction of the probed system. Furthermore time-dependent polarization states are used for example to generate SAP pulses via the polarization gating technique [25]. A full characterization of the driving IR pulse could allow for improving the generation of SAPs through the optimization of the time-dependent polarization.

2. Setup

Our setup (Fig. 1) consists of two main parts: the extreme ultraviolet (XUV) front-end, which provides SAPs, and a reaction microscope (or COLTRIMS) [26], which records the fragments of the ionization caused by the SAP in a gas target. The front-end's XUV-IR pump-probe interferometer is driven by a commercial CEP-stabilized [6] few-cycle Ti:sapphire laser system with a repetition rate of 10 kHz, pulse energy of 400 μJ, and a hollow-core fiber pulse compressor [27] generating pulses of about 5 fs, which were characterized by SPIDER measurements. The short intense IR pulses at high repetition rates are necessary for the generation of
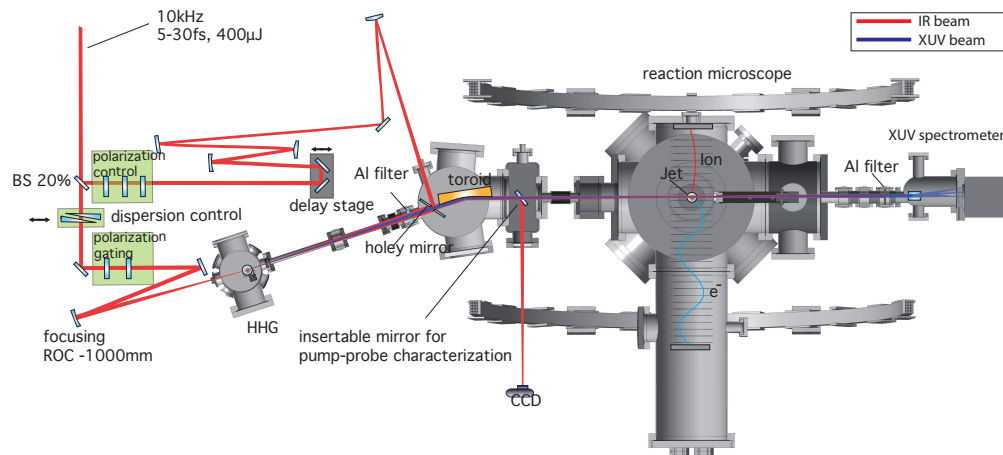
Fig. 1. Schematic of the setup with the XUV front-end on the left and the reaction microscope on the right.

SAPs with sufficiently high flux in order to allow for measurements with enough statistics in reasonable data acquisition times. SAPs are generated in an argon gas target by the use of a polarization gate [25] in one arm of the interferometer. Here, the polarization of the driving IR pulse is shaped such that it is linearly polarized only for one half-cycle, but elliptically polarized otherwise. Only during the time interval, called the gate, where the pulse is linearly polarized, ionized electrons can recollide with their parent ion and therefore emit a SAP via high-harmonic generation.

A 300 nm thick aluminum filter approximately compensates for the intrinsic chirp of the XUV pulses and removes the co-propagating IR. After recombination of the XUV with the delayed IR probe through a holey mirror, both beams are collinearly focused by a toroidal mirror into the supersonically expanded gas target of the reaction microscope. In order to maintain long-term stability, the driving laser beam pointing is stabilized prior to the pump-probe interferometer.

In the reaction microscope, ions and electrons are separated by the electric field of biased metallic plates and guided towards space and time sensitive detectors, allowing for the reconstruction of the 3D-momentum vector of each individual particle. By recording ions and electrons in coincidence, electrons arising from background ionization can be discarded from the data by placing filter criteria on the momentum sum of ions and electrons, thus increasing the signal quality.

XUV spectra are monitored throughout the measurements with a XUV spectrometer mounted on the rear side of the reaction microscope. Secondary events from XUV radiation are reduced by optimizing the dump geometry in front of the XUV spectrometer, therefore increasing the signal-to-noise ratio and ensuring the coincidence capabilities of the detector. The 10 kHz repetition rate allows for reasonably fast acquisition time with one or fewer events per laser shot.

3. Experiment

In order to extract the instantaneous amplitude and direction of the laser electric field with sub-cycle resolution, we perform an attosecond streaking experiment. Conventionally, streaking measurements have been performed with detectors that do not resolve the angular distribution of the photoelectrons, thus limiting the momentum resolution to only one dimension, which is compatible only with pure linearly polarized IR pulses [12, 13]. Velocity map imaging (V-

MI) could in principle address the momentum distribution along the polarization plane when extending it by tomographic reconstruction [28, 29]. Although, performing tomographic reconstruction at each delay step and rotating the IR polarization state in front of the toroidal mirror without distorting it, would remain challenging. The reaction microscope, instead, allows for the direct measurement of the full two-dimensional streaking trace along the *x* and *y* axis in the polarization plane of the propagating IR beam (see Fig. 2), thus directly supporting even time-dependent ellipticity and orientation of the IR pulses. Likewise classical streaking, the technique does not resolve spatial dependencies of the laser pulse, since the spatially averaged effective field, experienced by the target, is determined.

In a first experiment an elliptically polarized few-cycle IR pulse with time-independent ellipticity, hereafter referred to as polarization state 1 (PS1), is obtained by inserting a $\lambda/4$-plate in the beam path of the probe pulse. The corresponding streaking experiment is conducted with an argon gas target. Already the characterization of such a rather simple polarization state directly at the target is of great importance, e.g. for circular streaking experiments using the attoclock [15, 30, 31] and circular dichroism experiments in the multiphoton regime [32].

In a second experiment, conducted with a neon target, a more complex pulse shape with a time-dependent polarization state, hereafter referred to as polarization state 2 (PS2), is generated by a 205 µm thick birefringent quartz crystal plate oriented at an angle of 45° followed by a $\lambda/2$-plate placed at an angle of 22.5° relative to the linearly polarized laser. Different gases were employed to show that the technique does not rely on a specific target. Before reaching the target, the pulse traverses multiple optics, such as silver mirrors, a fused silica window, and the focusing toroidal mirror in grazing incidence. These optics will additionally modify the polarization state of the pulse and therefore with this technique we can characterize the time-dependent electric field vector of the pulse directly at the target.

The SAP, polarized along *x*, and the IR pulse are collinearly overlapped in the interaction region of the target and the IR pulse is sampled with the SAP by changing the delay τ in steps of 200 as. Negative delays correspond to the IR pulse arriving before the SAP. At a given delay τ, the SAP ionizes an electron and places it into the continuum with an initial momentum $p_0 = \sqrt{2(E_{SAP} - I_p)}$, with ionization energy I_p of the target gas, and central photon energy E_{SAP} (atomic units are used throughout this paper if not otherwise stated). The exact distribution of p_0 is governed by the orientation of the polarization, the spectrum of the XUV pulse, and the differential cross-section of the ionized target.

4. Analysis

From the moment of ionization until the end of the pulse, the electron is exposed to the driving force of the electric field of the IR pulse and acquires final momentum $p_{final}(\tau)$ (see Figs. 2 and 3):

$$p_{final}(\tau) = p_0 + \int_\tau^\infty F(t)\, dt = p_0 - \int_\tau^\infty E(t)\, dt = p_0 - A(\tau) \qquad (1)$$

By fitting a Gaussian function to a cut of the momentum distribution at any given delay τ and taking the peak position we obtain $p_{final}(\tau)$, which directly corresponds, except for a constant offset p_0, to the vector potential $A(\tau)$ at the moment of ionization (Eq. (1)). Note that the single photon ionization exhibits a small but finite delay [33, 34]. We recently could show that this time delay is in agreement with the predicted difference for argon and neon [35, 36]. However, the delay is in the range of tens of attoseconds and just shifts the zero position of the delay axis which is not determined anyway. We therefore can neglect this delay for this pulse characterization.

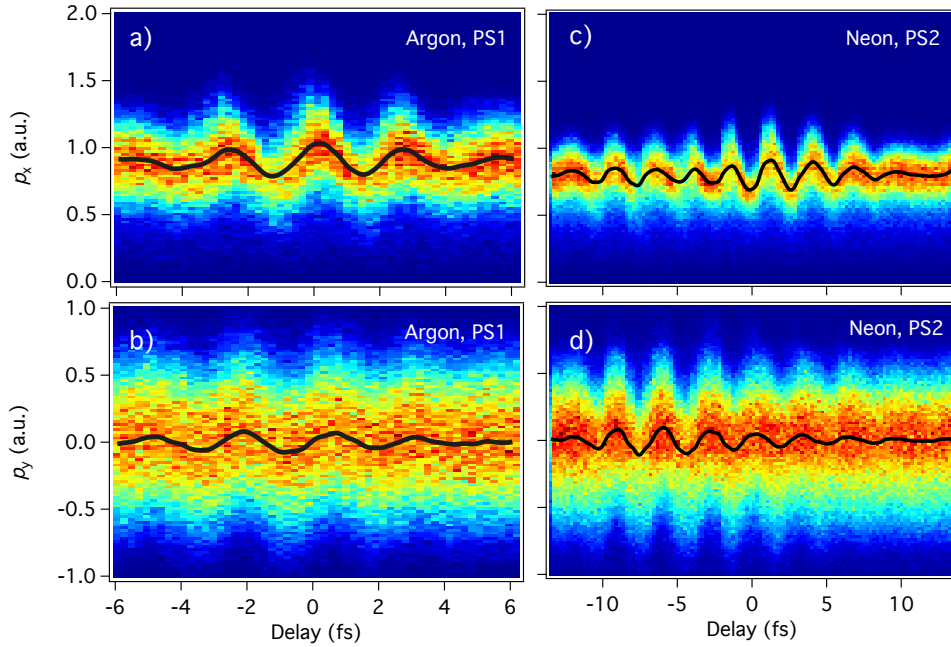We extract the peak of the distribution, as it is less sensitive to unstreaked background events,

Fig. 2. Streaking traces of a pulse with PS1 along p_x (a) and along p_y (b) overlapped with the extracted time-dependent momentum shift for each delay (black solid line), together with the streaking traces of a pulse with PS2 along p_x (c) and along p_y (d). For the definition of PS1 and PS2 refer to text.

which will result in artificially reduced amplitude when using a center-of-mass analysis. As we have access to the full momentum space in 3D, we can reconstruct $p_{\text{final}}(\tau)$ along the x and y axis of the polarization plane, thus, fully characterizing the laser pulse. Now, we directly obtain the electric field $E_{x,y}^{\text{Exp.}}(\tau)$ at the target from Eq. (2) (see Figs. 4 and 5).

$$E^{\text{Exp.}}(\tau) = -\frac{\mathrm{d}p_{\text{final}}(\tau)}{\mathrm{d}\tau} \qquad (2)$$

For the first experiment using the elliptically polarized pulse with PS1, we obtain the constant orientation $\theta = -22°$ and ellipticity $\varepsilon = 0.52$ of the polarization ellipse by fitting Eq. (3) to the data, see Fig. 5(a).

$$
\begin{aligned}
E_x(\tau) &= -f(t)E_0/\sqrt{2}\left[\cos\beta\sin(-\omega\tau - \theta) + \sin\beta\sin(-\omega\tau + \theta)\right] \\
E_y(\tau) &= -f(t)E_0/\sqrt{2}\left[\cos\beta\cos(-\omega\tau - \theta) - \sin\beta\cos(-\omega\tau + \theta)\right]
\end{aligned}
\qquad (3)
$$

The pulse envelope is described by $f(t)$. The other variables are the maximum of the electric field strength E_0, the orientation of the ellipse θ, and the ellipticity $\varepsilon = \cot(\beta + \pi/4)$.

Additionally, we investigate the time-dependence of the ellipticity $\varepsilon(\tau)$ and the orientation $\theta(\tau)$, defined by the amplitude and phase of two perpendicular fields [37]:

$$\varepsilon(\tau) = \tan\left[\frac{1}{2}\sin^{-1}\left(\frac{2E_x(\tau)E_y(\tau)\sin(\phi_x(\tau) - \phi_y(\tau))}{|E_x(\tau)|^2 + |E_y(\tau)|^2}\right)\right] \qquad (4)$$
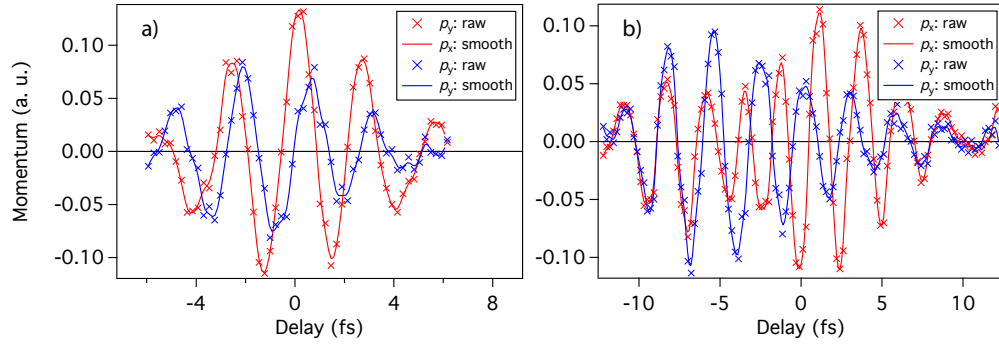
Fig. 3. Momentum shift along the x (red) and y axis (blue) for each delay step with raw data (crosses) and smoothed data (solid lines) for PS1 (a) and PS2 (b). p_0 was removed from $p_{\text{final}}(\tau)$ along the x axis to center both curves at zero. For the definition of PS1 and PS2 refer to text. Henceforth, the smoothed data are used.
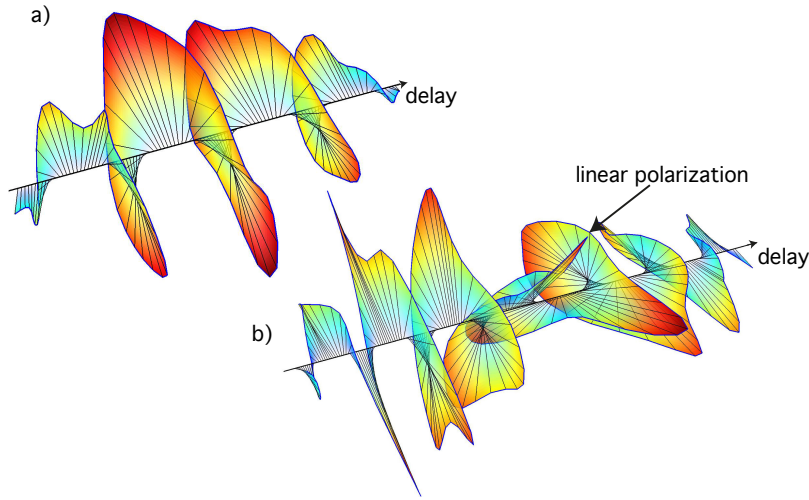

Fig. 4. Visualization of the temporal behavior of the pulse electric field for PS1 (a) and PS2 (b). In (b) one can clearly see a change in helicity with a linear part in the center of the pulse.

$$\beta(\tau) = \frac{1}{2} \tan^{-1} \left[\frac{2E_x(\tau)E_y(\tau)\cos\left(\phi_x(\tau) - \phi_y(\tau)\right)}{|E_x(\tau)|^2 - |E_y(\tau)|^2} \right] \tag{5}$$

where the time-dependent amplitude and temporal phase of the complex electric field are given by $E_{x,y}(\tau)$ and $\phi_{x,y}(\tau)$, respectively. The experiment, however, measures the real part of the electric field from which we extract the time-dependent envelope and phase by applying a Gabor analysis with the window width adjusted to cover one optical cycle of the IR. Finally, we obtain the time-dependent ellipticity by inserting the extracted amplitude and phase into Eq. (4) (see Fig. 5).
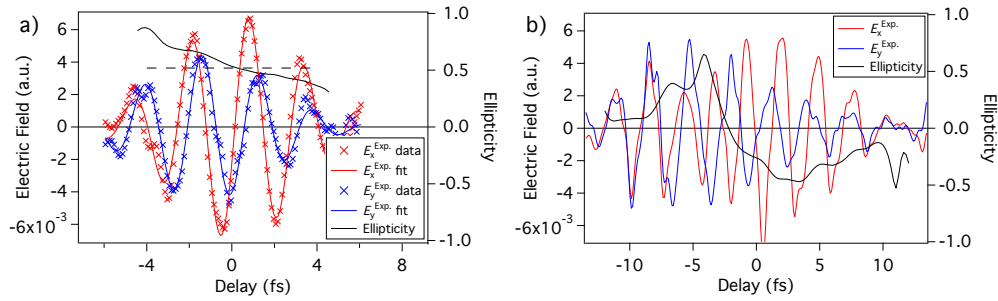
Fig. 5. Electric field along the *x* and *y* axis (red and blue crosses, respectively), fit of analytical expression of elliptically polarized pulse along *x* and *y* axis (red and blue solid lines, respectively), instantaneous ellipticity (black solid line), and $\varepsilon = 0.52$ from fit (dashed black line) for elliptically polarized pulse (PS1) (a). Note how the ellipticity is not constant but slightly varies over the pulse duration. Measured electric field along *x* and *y* axis (red and blue solid lines, respectively) and time-dependent ellipticity (black solid line) for the pulse with PS2 (b). Here, the changes in the ellipticity are more pronounced, it even changes sign indicating the change of helicity of the pulse. In the region of the sign change, the polarization becomes linear.

5. Results

With this approach we can directly observe the evolution of the ellipticity over time. In Fig. 5(a) we see that the ellipticity of the pulse with PS1 is not perfectly constant as one could have expected, but varies slightly around the value obtained from the fit. The slight time-dependence of the ellipticity occurs because of the large, more than 300 nm bandwidth of our pulses in conjunction with its residual chirp and the chromatic errors of our waveplate. Any time-integrating method for characterizing the polarization would not be suitable in this case. When averaging the ellitpticity over the pulse duration, weighting it with the amplitude of the electric field, we obtain $\varepsilon = 0.50$ as compared to $\varepsilon = 0.52$ from the fit.

   In Fig. 5(b) we see the more complex shape of the pulse with PS2 generated for the second experiment. Not only do we observe a pronounced variation in the ellipticity, but also a change in the helicity from left-handed (positive ε) for negative delays to right-handed (negative ε) for positive delays. A short linear part at the center of the pulse, where the ellipticity is close to zero, reveals a polarization state very similar to the one used with the polarization gating technique mentioned before. The change in ellipticity goes together with the phase slip of $E_x^{\text{Exp.}}$ with respect to $E_y^{\text{Exp.}}$ along the delay axis as can be seen in Fig. 5(b).

6. Conclusion

In conclusion, we have demonstrated a full characterization of the time-dependent electric field vector of an IR laser pulse in the polarization plane using a 2-dimensional attosecond streaking technique. We are able to measure the orientation and absolute amplitude of the vector potential, and thus the electric field, with sub-cycle resolution over the complete pulse directly at the target. This allows for the calculation of the ellipticity and orientation of the IR pulse for any instant of time within the pulse. To the best of our knowledge, this is not possible with any other existing pulse characterization method.